Journal of Membrane Science 526 (2017) 355–366

Contents lists available at ScienceDirect

Journal of Membrane Science

journal homepage: www.elsevier.com/locate/memsci

TpPa-2-incorporated mixed matrix membranes for efficient water purification

Lina Xu, Jia Xu*, Baotian Shan, Xiulin Wang, Congjie Gao

Key Laboratory of Marine Chemistry Theory and Technology, Ministry of Education, College of Chemistry and Chemical Engineering, Ocean University of China, Qingdao, Shandong 266100, China

ARTICLE INFO

Keywords:
Mixed matrix membrane
Covalent organic frameworks
TpPa-2
Water treatment
Trade-off effect

ABSTRACT

Pure organic nature and nanoporous structure make covalent organic frameworks (COFs) a promisingly potential candidate in mixed matrix membranes (MMMs). However, COFs-based MMMs have hardly ever been applied in water purification due to their hydrolytic nature. In this study, we elaborately selected TpPa-2 with extensive stability in complicated water-environments as nanofiller to prepare MMMs for water treatment for the first time. Microwave synthetic technique was employed and optimized to construct the TpPa-2(MW) with a much higher BET surface area, smaller particle size, less agglomeration tendency and excellent stability. TpPa-2 was also synthesized mechanochemically (MC) for comparison to indicate how the synthetic technique influences the TpPa-2 and TpPa-2-incorporated MMMs. Membrane structure and property, water transport capacity and separation performance of both TpPa-2(MW)- and TpPa-2(MC)-incorporated MMMs were comprehensively investigated. It proved that our MMMs with an ultralow amount (0.2 wt%) of TpPa-2(MW) featured both improved water flux and rejection, breaking the trade-off between permeability and selectivity for polymer membrane. A membrane forming mechanism was further proposed to understand the effectiveness of TpPa-2(MW) in MMMs. This new generation COFs-based MMMs would be highly efficient, resource saving and cost-effective, which promise a great potential application in practical water purification.

1. Introduction

Dwindling fresh water resources and increasing water contamination nowadays are generating a significant demand on the development of water treatment technologies. Membrane separations have provided safe water supply in a more energy efficient and environmentally sustainable way and played an increasingly significant role in areas such as drinking water supply, seawater desalination and wastewater reclamation [1]. Existing membranes for water treatment, typically polymeric in nature, have particular advantages on decent separation performance, excellent flexibility, low cost, easy processability and scale-up manufacture [2,3]. However, due to the glassy backbone and interchain packing of polymeric materials [4,5]. the inherent trade-off relationship between permeability and selectivity [5] limits the separation performance of polymeric membranes and their further applications. The development of membranes with both high permeability and rejection is urgently desired for water purification under the context of energy efficiency and cost effectiveness.

Mixed matrix membranes (MMMs), an advanced class of membranes with nanomaterials dispersed in their polymeric matrices, are emerging as a promising solution to overcome the trade-off relationship originally in the field of gas separation in the 1990s [6]. Recently, MMMs have achieved a significant potential in water treatment to be a next generation of high performance membranes [7] where inorganic nanofillers such as silica [8], TiO_2[9], carbon nanotubes (CNTs) [10–12] carbon molecular sieve (CMS) [13] and metal-organic frameworks (MOFs) [14,15] are incorporated into polymers to improve both permeability and rejection [16,17]. However, among state-of-the-art MMMs for water treatment, some challenges are still needed to be addressed [7]: (1) nanofillers with less agglomeration in the host polymer and more extensive stability in complicated water environments are highly desired [18]; (2) the unsatisfactory interfacial

Abbreviations: COFs, covalent organic frameworks; S_{BET}, Brunauer-Emmett-Teller surface area; Tp, 1,3,5-triformylphloroglucinol; Pa-2, 2,5-dimethyl-p-ph-enylenediamine; GAA, glacial acetic acid; TpPa-2, sythesized by solvothermal method; TpPa-2MC, TpPa-2 sythesized by mechanochemical method; TpPa-2 MW, sythesized by microwave method; DMAC, Dimethylacetamide; PEG, polyethylene glycol; HA, humic acid; PSf, Polysulfone; TpPa-2(MW)/PSf, the mixed matrix membrane prepared with TpPa-2(MW) and PSf; TpPa-2MC/PSf, the mixed matrix membrane prepared with TpPa-2(MC) and PSf; FTIR, Fourier-transform infrared spectroscopy; PXRD, powder X-ray powder diffraction; SEM, scanning electron microscopy; DFT, Density Functional Theory (DFT); Lp, pure water permeability; J, permeation flux; R, rejection

* Corresponding author.
E-mail address: qdxujia@sina.com.cn (J. Xu).

http://dx.doi.org/10.1016/j.memsci.2016.12.039
Received 8 October 2016; Received in revised form 15 December 2016; Accepted 20 December 2016
Available online 21 December 2016

compatibility between nanomaterials and polymeric matrix hinders the stability of nanomaterials within the host polymer due to the inorganic nature of nanomaterials. All of them would lead to severe looseness and even leakage of nanofillers and thus compromise the optimal separation performance and operational durability [19]. It is also no exception for MOFs, although they possess organic-inorganic hybrid structure [15]. The relatively poor stability for most MOFs in water and acid conditions limited their application in water purification [20,21]. Therefore, a pure organic nanofiller might be a good choice for highly stable and efficient MMMs applied in water treatment.

Covalent organic frameworks (COFs), emerged as a novel family of nano-porous materials, have received considerable interest in recent years since firstly reported in 2005 [22]. The pure organic nature of COFs might potentially provide good compatibility and dispersion with polymeric matrices to fabricate an efficient MMMs. Recent work has verified the effectiveness of COFs incorporation on the filler-polymer compatibility and the effectiveness of improved compatibility on the superior separation performance [23]. For example, Shan et al. prepared ACOF-1-based MMMs with 16 wt% ACOF-1 for gas separation, which showed a more than two times of CO_2 permeability and a slight increase in selectivity compared to the pure polymer membrane without ACOF-1 [24]. However, typical COFs including COF-1 [22], COF-5 [22], COF-108 [25] and COF-202 [26], usually synthesized based on a reversible organic reaction such as boronic acid trimerization [22,27] and boronate ester formation [23,27], can decompose easily and completely even in the case of ambient humidity [28,29], which restrict their applications in water environment [27]. Therefore, there is, up to now, no any report on the COFs incorporated MMMs for water purification, although most COFs have been investigated in widely fields of gas storage [30,31], catalyst [32], optical imaging and sensory [33].

Recently, TpPa-1 and TpPa-2 (Fig. 1) synthesized by the Schiff base aldehyde-amine condensation reaction of 1,3,5- triformylphloroglucinol (Tp) with p-phenylenediamine (Pa-1) or 2,5-dimethyl-p-phenylenediamine (Pa-2) [34,35] exhibit a strong hydrolytic stability, which might possess a huge potentiality in MMMs. Banerjee et.al. [36] fabricated MMMs comprising TpPa-1 for gas separation, which exhibited an exciting enhancement in permeability with appreciable separation factors due to the improved compatibility of TpPa-1 with polymer (PBI-BuI) matrix and the pore modulation of TpPa-1. However, although TpPa-1 was successfully used in gas separation [34,35,37], where the requirement of hydrolytic property is less rigorous, unfortunately TpPa-1 exhibits a structural instability at higher pH [34,35], limiting its application in water treatment because membranes are exposed to the complicated feed with a large number of pollutant during filtration and even acid/alkaline solutions when chemical cleaning is performed for the removal of membrane fouling. By contrast, TpPa-2 might be a more appropriate choice to fabricate MMMs for water purification due to its exceptional hydrolytic and chemical stabilities in extensive pH range.

However, TpPa-2 suffered from a lower Brunauer-Emmett-Teller (BET) surface area (S_{BET}) of less than 300 m^2/g compared to TpPa-1 with S_{BET} of ~724 m^2/g, probably compromising its effectiveness and feasibility in MMMs. And, the conventional routes to synthesize TpPa-2, such as solvothermal (ST) and mechanochemical (MC), required a time-consuming and complicated operation [34,35]. Hence, the improvement in S_{BET} of TpPa-2 via a facile and efficient way is a key point in highly efficient MMMs for water treatment. Microwave (MW) technique is of considerable interest in modern synthetic chemistry [38] to synthesize cuprous oxide [39], inorganic zeolite [40], MOFs [41,42] and COFs [37,43,44]. It proves to improve the S_{BET}[41] and shorten the synthetic period [42]. For example, the S_{BET} of TpPa-1 increased from 535.0 to 724.6 m^2/g when using a microwave approach [34,37]. Therefore, we believe that microwave technique is more suitable to synthesize TpPa-2 with an improved nanostructured property.

Inspired by the unique nature of TpPa-2 and relative pioneering studies, we devoted efforts for the first time, in the tailored fabrication of high-efficient MMMs comprising TpPa-2 for water purification. The organic nature of TpPa-2 will enhance the compatibility between nanofiller and polymeric matrix and ensure better dispersion at a molecular level, and its hydrolytic stability can facilitate the membrane operational durability and efficiency in water environment. In this study, a more effective and simplified microwave approach was developed to construct TpPa-2 with higher S_{BET}, improving the separation performance of MMMs. In order to modulate the nanostructure of TpPa-2, MW conditions were optimized and another synthesis approach such as mechanochemical approach was also employed for comparison. The membrane structure and separation performance of the resulting TpPa-2-incorporated MMMs were investigated to evaluate the effectiveness of different synthetic approach of TpPa-2. Moreover, a separation mechanism for the TpPa-2-incorpo-

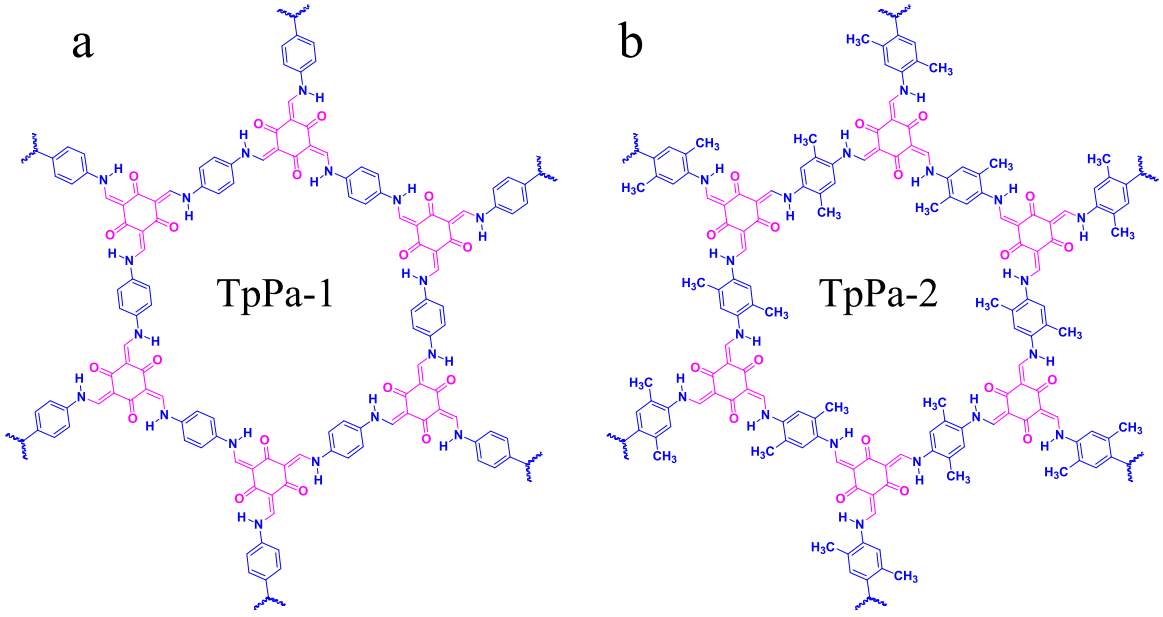

Fig. 1. Chemical structures of (a) TpPa-1 and (b) TpPa-2.

rated MMMs was proposed accordingly to understand the effect of TpPa-2 on the synchronous improvements in water permeability and solute rejection during water purification.

2. Experimental section

2.1. Chemicals

All the chemicals were used as received. Hexamethy-lenetetramine (≥99%, Sigma-Aldrich), phloroglucinol (Sigma-Aldrich), trifluoroacetic acid (99%, Sigma-Aldrich), 2,5-dimethyl-1,4-phenylenediamine (Pa-2, > 98%, TCI), dioxane (≥99.5%, Aladdin), mesitylene (98%, Sigma-Aldrich), dichloromethane (99.5%, Aladdin), dimethylacetamide (DMAc, Sinopharm), polyethylene glycol (PEG, 400 Da, Sinopharm), hydrochloric acid (HCl, 36–38 wt%, Sinopharm), humic acid (HA, Sigma), polysulfone (PSf, Udel P-1700, USA), glacial acetic acid (GAA, Sinopharm), anhydrous acetone (Sinopharm). Raw seawater was collected from the Yellow Sea, China.

2.2. Microwave synthesis of TpPa-2

A simplified microwave reactor (XH-MC-1, Xianghu, China) with a contact temperature probe was employed for the TpPa-2 synthesis (Fig. 2). The reaction equation was also shown in Fig. 2. Microwave synthesis of TpPa-2 was carried out based on modified Schiff base reactions. Initially, Tp, as intermediate material of TpPa-2 was prepared from phloroglucinol [34,35,45] (Supporting Information). Then, in the presence of 3 M GAA (2.5 mL) and a mixed solvents of mesitylene/dioxane (1:1, 15 mL), Tp (1.5 mmol) was reacted with Pa-2 (2.25 mmol) to synthesize TpPa-2 based on the modified Schiff-base reactions, which was carried out in an open microwave system with microwave power of 500 W at a predetermined temperature (100 °C, 120 °C) for a certain time (30, 60 and 90 min). Finally, the mixture were collected by centrifugal separation and extracted by acetone (100 mL) for 60 min with 4 cycles for purification under ambient condition. Before measuring porosity and S_{BET}, the samples were degassed at −196 °C and activated at 180 °C for 6 h under high-vacuum conditions. The resultant TpPa-2 was denoted as TpPa-2(MW). For comparison, TpPa-2 was also prepared using mechanochemical method (denoted as TpPa-2(MC)) by manual grinding in a mortar and pestle, similar to the previous studies [35]. TpPa-2(MC) was initially identified by visual color change (Fig. S1b).

2.3. Evaluation of hydrolytic and chemical stabilities of TpPa-2

In order to expand the application of TpPa-2(MW) into water treatment, it was of utmost importance to probe comprehensively into the hydrolytic and chemical stabilities of TpPa-2(MW) in the more complicated solution environment. In this study, deionized (DI) water, strong acid (concentrated HCl solution, 36–38%), harsh base (saturated NaOH solution, 20 M), organic solvent (n-hexane) and natural seawater (salinity of ~3.5%) were selected as representative solutions. TpPa-2(MW) samples were dosed into various solutions for 7 days. Subsequently, FTIR, PXRD and SEM measurements were conducted to evaluate its changes in the chemical composition, crystallinity and morphology.

2.4. Fabrication of TpPa-2-incorporated MMMs

TpPa-2 were blended with PSf to prepare MMMs via non-solvent induced phase inversion [46,47]. 0.2 wt% TpPa-2 (in total casting solution) was firstly added into DMAc followed by ultrasonication for 1 h to achieve good dispersion. PSf (18 wt%) and PEG400 (8 wt%) were then added into the TpPa-2-containing DMAc solution followed by stirring for at least 24 h at 60 °C until a homogeneous casting solution was obtained. The casting solution was then degassed overnight and then cast onto a glass plate using a casting knife with a thickness of 150 μm. The casting film was immersed into DI water bath at room temperature for 12 h and finally stored in DI water before use. The resultant TpPa-2-incorporated membranes were denoted as TpPa-2(MW)/PSf and TpPa-2(MC)/PSf membranes. As control, pure PSf membrane without TpPa-2 was also fabricated under the same fabricating procedure.

2.5. Characterization of TpPa-2 and TpPa-2-incorporated MMMs

Fourier-transform infrared (FTIR) spectroscopy was performed to evaluate the chemical composition of TpPa-2 using Tensor 27 spectrometer (Bruker, Germany). Powder X-ray diffraction (PXRD) was determined to evaluate the crystallinity of TpPa-2 using D8 ADVANCE diffractometer (Bruker, Germany), equipped with a Cu Kα radiation source (λ=1.5418 Å). Scanning electron microscopy (SEM) was used to observe morphology of TpPa-2 using S-4800 scanning electron microscope (Hitachi, Japan) at 15 kV. Particle size distribution of TpPa-2 was determined using dynamic laser scattering equipment (Zetasizer Nano S90, Malvern, England) by uniform dispersion of TpPa-2 in DMAc to evaluate the dynamic aggregation of TpPa-2 in casting solution. Porosity and S_{BET} was measured by N_2 adsorption-desorption isotherms profiled at −196 °C after being degassed and activated at 180 °C for 6 h under high-vacuum conditions. Pore size distribution of TpPa-2 was evaluated using Density Functional Theory (DFT) method.

For the membrane characterization, SEM and FTIR were employed to evaluate the morphology and chemical composition, respectively. Pore size distribution of membranes was determined via membrane pore size analyzer (3H-2000PB, BeiShiDe, China) based on bubble pressure method. Membrane sample was soaked in Porofil overnight before test. Thickness meter (Liuling, China) was used to determine the membrane thickness. Surface hydrophilicity was measured using a contact angle instrument (DSA 100, Kruss, Germany). 10 different locations were selected and the average value was calculated in order to decrease the experimental error. Water uptake (WU) and porosity (ε) of membranes were determined by gravimetric method, respectively. Membrane sample was soaked in DI water for 24 h and weighed after

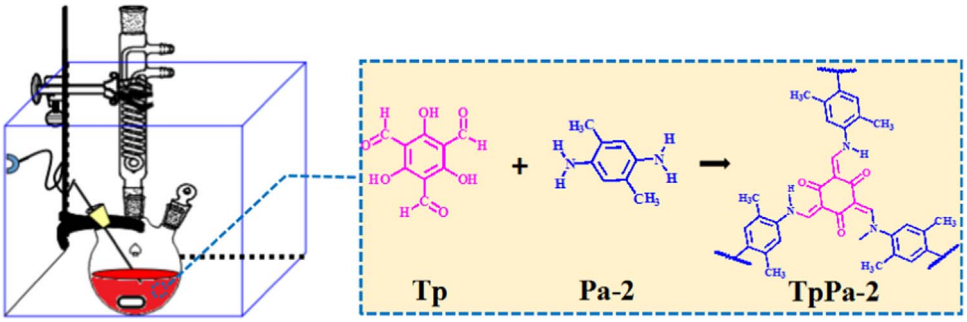

Fig. 2. Schematic diagram of experimental apparatus and chemical reaction of TpPa-2(MW).

removing the excess water on the surface using tissue paper. Then the wet sample was dried in a vacuum oven at 40 °C for 24 h and weighed again. WU and ε were calculated by the following Eqs. (1) and (2).

$$WU = \frac{m_w - m_d}{m_d} \times 100\% \quad (1)$$

$$\varepsilon = \frac{m_w - m_d}{\rho d A} \times 100\% \quad (2)$$

where m_w and m_d are the wet mass and dry mass of MMMs, respectively. ρ is the density of water (1.0 g/cm^3) at 25 °C. A and d are the surface area (cm^2) and the thickness (cm) of the wet membranes, respectively. It was assumed that all the pores in the membrane and TpPa-2 were completely filled with water.

2.6. Evaluation of water transport property and separation performance of TpPa-2-incorporated MMMs

In this study, water transport property was characterized by pure water permeability (*L*p), which was measured using a homemade cross-flow UF setup with an effective membrane area of 20 cm^2. The membrane sample was pre-pressurized with DI water at 0.15 MPa for 2 h until reaching a steady permeation state. Then *L*p was measured at the four trans-membrane pressures of 0.08, 0.1, 0.12, 0.14 and 0.16 MPa [47], which was repeated at least three times to obtain average value. *L*p can be calculated by Eq. (3).

$$L_p = \frac{Q}{AtP} \quad (3)$$

where *Q* is the quantity of the permeate sample collected over a period of time (L); t is the time of permeation (h); A is the effective membrane area for filtration (m^2); P is the transmembrane pressure (MPa).

Separation performance in terms of water flux (*J*) and HA rejection (*R*) was evaluated via UF experiments in dead-end and constant-pressure mode at 0.10 MPa and room temperature [48]. HA solution was employed as a representative organic foulant feed and each UF test was conducted for 120 min *J* and *R* can be calculated from Eqs. (4) and (5), respectively.

$$J = \frac{Q}{At} \quad (4)$$

$$R = \frac{C_f - C_p}{C_f} \times 100\% \quad (5)$$

where C_f and C_p are the HA concentrations in the feed and permeate, respectively, which are determined by a UV–vis spectrophotometer (UV-2450, Shimadzu, Japan) at the wavelength of 254 nm.

3. Results and discussion

3.1. TpPa-2 synthesis and optimization

TpPa-2(MW) and TpPa-2(MC) (as control) synthesized in this study were initially identified by visual color change from yellow to dark red (Fig. S1b and S3, Supporting Information). To better understand the chemical structure of TpPa-2(MW), FTIR was employed and compared the results with those for the TpPa-2(MC) synthesized by mechanochemically as well as the starting materials. As shown in Fig. 3a, compared with the starting material such as Tp and Pa-2, the peaks at approximately 3100–3300 cm^{-1} corresponding to the N–H stretching bonds of the free diamine in Pa-2, and the peak at approximately 1639 cm^{-1} corresponding to the C=O stretching bonds of carbonyl in Tp were disappeared and accompanied by an extra strong peak at 1580 cm^{-1} ascribing to C=C bonds and a new weak perk at 2889 cm^{-1} ascribing to C-H bonds in methyl group for the TpPa-2 obtained by microwave irradiation, indicating the complete consumption of Tp and Pa-2 and the existence of final keto form of TpPa-2(MW)

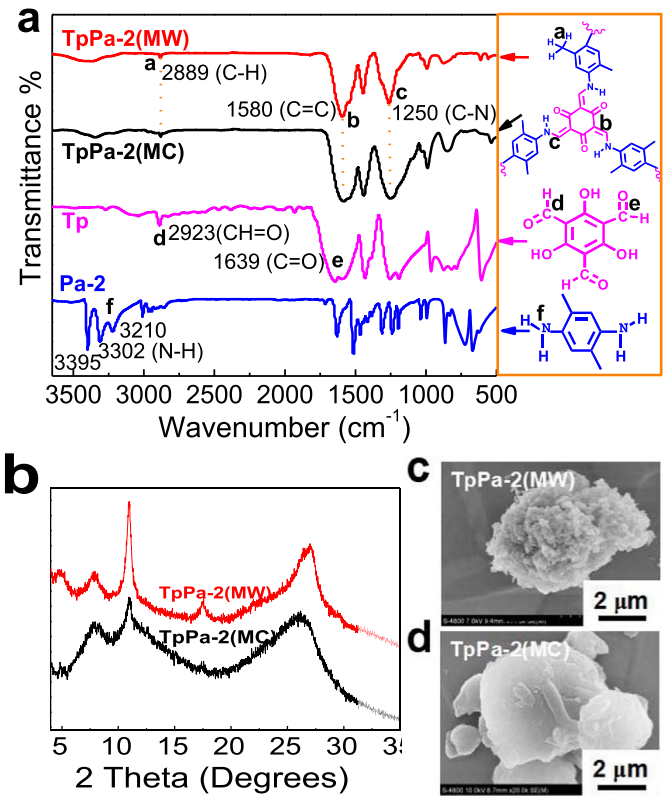

Fig. 3. Characterization of TpPa-2(MW) and TpPa-2(MC). (a) FTIR spectra of Tp, Pa-2, TpPa-2(MW) and TpPa-2(MC); (b) PXRD patterns of TpPa-2(MW) and TpPa-2(MC); SEM images of (c) TpPa-2(MW) and (d) TpPa-2(MC). TpPa-2(MW) was synthesized under 100 °C for 60 min.

[34]. It should be noted that the C=O peaks of TpPa-2(MW) at 1639 cm^{-1} were not observed, which might be merged with the C=C stretching band at 1580 cm^{-1}. These typical FTIR peaks of the resulting TpPa-2(MW) and TpPa-2(MC) in this study matched well with TpPa-2 reported in previous studies [34,35], which confirmed the successful synthesis of TpPa-2 by microwave irradiation.

Powder X-ray diffraction (PXRD) patterns (Fig. 3b) of TpPa-2(MW) exhibited four strong peaks at 2θ=4.7°, 7.9°, 14.5° and 26.5°, showing a moderate crystallinity. In comparison with the TpPa-2(MW), the first perk at 2θ=4.7°, corresponding to the (100) reflection plane, was relatively less intense for TpPa-2(MC), which might be due to the random displacement of the 2D layers during the mechanochemical exfoliation, resulting in hindering the pore accessibility and weakening the reflection corresponding to the (100) plane [35]. It demonstrated that a more complete and uniform crystalline structure of TpPa-2 could be achieved by microwave route. It could be explained considering by the promoted reaction temperature in seconds triggered by electromagnetic field, which could effectively boost the formation and growth of crystal nucleus [38,41,49]. A broad peak at higher 2θ (~26.5°), corresponding to the (001) reflection plane, was obtained for both TpPa-2(MW) and TpPa-2(MC) due to the π–π stacking between the TpPa-2 layers. The π–π stacking distance between two layers was calculated to be 3.35 Å from the d spacing based on Bragg equation, which matched well with the distance results of the reported TpPa-2 synthesized solvothermally and mechanochemically [34,35].

SEM images of TpPa-2(MW) showed a spherical-like morphology with zigzag margin and loose nanostructure (Fig. 3c), which would enlarge the surface area of material and thus improve its separation and absorption efficiency, whereas TpPa-2(MC) presented a heaped-up structure in the form of bulk powder agglomerates (Fig. 3d), which was consistent with the reported TpPa-2(MC) [35]. It indicated that the microwave synthesis facilitated to construct porous and uniformly

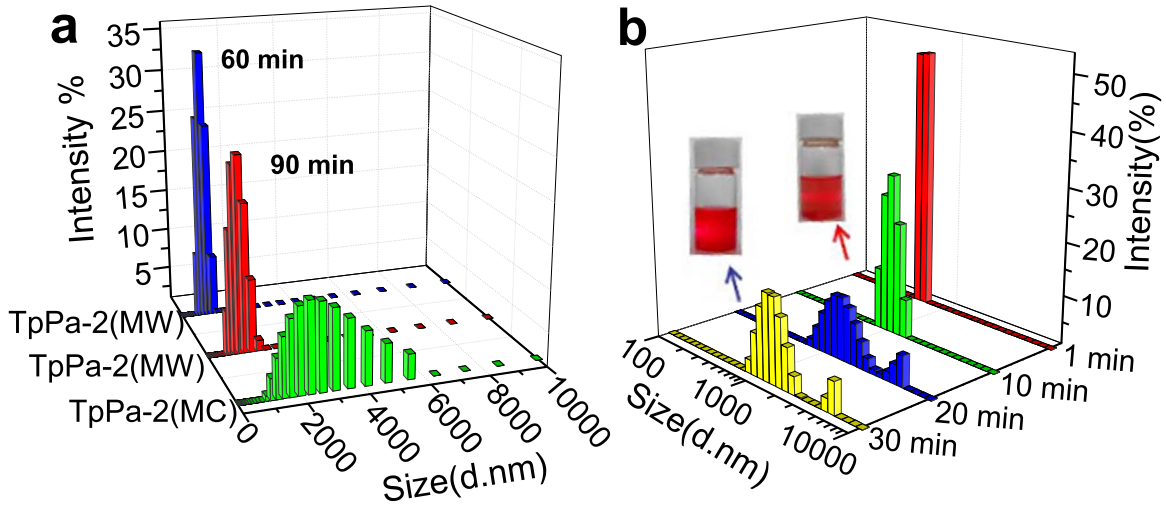

Fig. 4. Dynamic laser scattering measurements for TpPa-2. (a) Particle size distributions of TpPa-2(MC) and two TpPa-2(MW) prepared at 100 °C for 60 and 90 min, respectively; (b) change in particle size distribution with time of TpPa-2(MW) prepared at 100 °C for 60 min.

nanostructured TpPa-2.

Dynamic laser scattering (DLS) measurements (Fig. 4a) revealed that TpPa-2(MW) performed a narrow distribution with an average particle diameter of ~500 nm, while TpPa-2(MC) displayed a broader and more uneven distribution with a larger average diameter of ~3 μm, similar to that of TpPa-2(MC) prepared by Banerjee group [35]. It indicated that microwave irradiation tended to synthesize smaller TpPa-2 crystals, which could be attributed to the fast production of hot spots due to the reactant dissolution within short time under a quick and uniform superheating by electromagnetic field, leading to the nucleation/crystal growth at both enhanced rate and concentration which facilitate the formation of small crystals [50,51]. However, even for the TpPa-2(MW) with smallest initial particle size, self-agglomeration phenomenon occurred inevitably when exposed to solvent. In order to evaluate the agglomeration behavior of TpPa-2(MW), the dynamic agglomeration process was investigated via DLS measurements. As illustrated in Fig. 4b, initially well-dispersed TpPa-2(MW) with DMAc as solvent exhibited an average particle size of ca. 500–600 nm and an apparent Tyndall effect, while after the exposure time of 20 min, Tyndall effect was weakened gradually and a broader particle size distribution along with an increasing particle size of 800–1200 nm was observed. With a further increase in exposure time to 30 min, there is no distinct difference in the particle size distribution. It indicated an intense agglomerating propensity of TpPa-2(MW) within approximately 20 min, which could make the particle size doubled. It was worth noting that even in this case, the particle size with a narrow distribution of the agglomerated TpPa-2(MW) was superior to that of the initially dispersed TpPa-2(MC), demonstrating the effectiveness of microwave irradiation on the reduction in particle size of TpPa-2.

Nitrogen adsorption-desorption experiments were performed to examine the permanent porosity of TpPa-2(MW) prepared at 100 °C for 60 min (Fig. 5c). It exhibited a typical type-I reversible isotherm. DFT fitting of the adsorption branches showed that the TpPa-2(MW) exhibited a pore size distribution ranged 1–10 nm with an average pore size of 1.41 nm (Fig. 5c, the insert), which matched well with the corresponding reported values of 1.35 nm for TpPa-2(ST) [34] and 1.5 nm for TpPa-2(MC) [35], demonstrating that various methods involving solvothermal, mechanochemical and microwave irradiation had little impact on the pore size of TpPa-2. Total pore volume at P/P_0=0.99 was calculated to be approximately 0.38 cm^3/g. Differently, the resulting TpPa-2(MW) yielded a dramatically improved S_{BET} up to 535.2 m^2/g (correlation coefficient=0.982, Fig. 5d and Fig. S2b), which was over one order of magnitude higher than the reported TpPa-2(MC) [35] and the synthesized TpPa-2(MC) in this work (61.6 m^2/g, correlation coefficient=0.999, Fig. 5d and Fig. S2e) and 1.6 times higher than the reported TpPa-2(ST) [34] (as seen Fig. 5d). The obtained high S_{BET} might be related to the small and homogenous TpPa-2(MW) crystals, in theory attributed to the high nucleation/crystal growth rate at the presence of microwave irradiation. Moreover, TpPa-2 was successfully synthesized at open system by microwave irradiation within 60 min, exhibiting a higher reaction rate of more than 72 times faster than that of the reported TpPa-2 prepared using solvothermal method (72 h) [34]. It also demonstrated that the over-pressure achieved by sealed tube [43] could not be employed in the synthesis of some COFs materials such as TpPa-2, which provided a more time-effective, operation-simplified and safer way to fabricate COFs materials at a large scale.

In order to evaluate the effect of microwave conditions on the structure and crystallinity of TpPa-2(MW), microwave temperature (100 and 120 °C) and time (30, 60 and 90 min) were investigated and optimized. According to the FTIR and PXRD measurements (Fig. 5ab), TpPa-2(MW) synthesized at different microwave temperature and time exhibited identical chemical composition and crystalline structure, which were in accordance with the reported TpPa-2(ST) in literature [34]. However, microwave conditions exerted a significant effect on the S_{BET} (Fig. 5d). At 100 °C for 30 min, the resulting TpPa-2(MW) yielded a lower S_{BET} of 130.6 m^2/g (correlation coefficient=0.999, Fig. 5d and Fig. S2a). It might be attributed to the existence of unreacted monomers or impurities trapped within the crystalline structures due to the shorter reaction time [31]. When prolonging reaction time from 60 to 90 min, TpPa-2(MW) emerged a sharply decrease in S_{BET} of 123.3 m^2/g (correlation coefficient=0.999, Fig. 4d and Fig. S2c), which might be attributed to continuous crystal growth with reaction time into larger particles with an average diameter of ~800 nm (Fig. 4a). The lowered S_{BET} under a longer reaction time was consistent with the literature [48]. Besides, the elevation of microwave temperature from 100 to 120 °C also played a negative impact on the S_{BET} of TpPa-2(MW), which was lowered to 145.2 m^2/g (correlation coefficient=0.999, Fig. 5d and Fig. S2d). It might be explained that higher temperature could induce amorphization via the partial framework collapse of porous crystalline TpPa-2 polymorphs and thus form a dense topologically disordered phase [52]. It was speculated that beyond the energy threshold or mechanical limit which existed in crystal synthesis, crystal-to-amorphous transition could occur [52–54], which was one of basic mechanisms for the synthesis of amorphous MOFs from their crystalline counterparts via drastic ball milling, overpressure, heating, and electrical discharge-induced methods [55–59]. Such amorphous MOFs facilitated their applications in the release

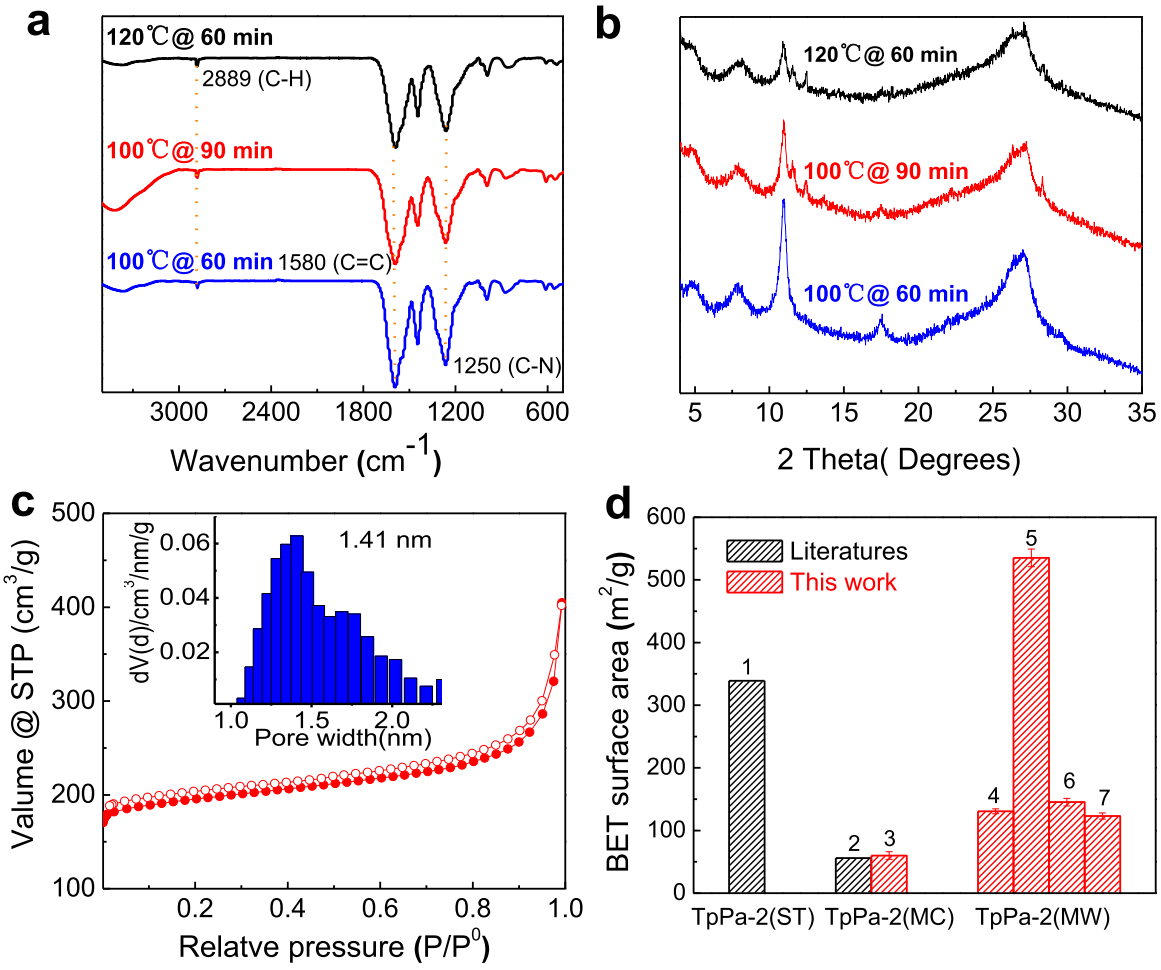

Fig. 5. Characterization of TpPa-2(MW) synthesized under various microwave conditions. (a) FTIR spectra and (b) PXRD patterns of TpPa-2(MW) synthesized at 100 and 120 °C for 60 and 90 min. (c) Nitrogen adsorption–desorption isotherms of TpPa-2(MW) synthesized at 60 min for 100 °C, and the inset plot presented its pore size distribution; (d) Summary of S_{BET} of TpPa-2 in literature and this work: (1) TpPa-2(ST) synthesized at 100 °C for 72 h in literature; (2) TpPa-2(MC) synthesized at 25 °C for 60 min in literature; (3) TpPa-2(MC) synthesized in this study, under the same condition as (2); (4–7) TpPa-2(MW) synthesized at 100 °C for 30 min, 100 °C for 60 min, 100 °C for 90 min and 120 °C for 60 min in this study, respectively.

and storage of reversible gas and harmful substance. However, the transition from crystal to amorphization could lead to dramatic reductions in both porosity and S_{BET} [58,59]. For the TpPa-2(MW), further increases in the reaction time (more than 60 min) and temperature (more than 100 °C) might trigger the coexistence of crystalline and amorphous TpPa-2, leading to a sacrifice in partial inherent channel of the crystalline TpPa-2 polymorphs and thus a less S_{BET}. Therefore, proper reaction time and temperature was so vital to mitigate the crystal-to-amorphous transition, resulting in an improved S_{BET} of TpPa-2(MW). TpPa-2 synthesized under optimal microwave condition of 100 °C for 60 min was adopted in the subsequent investigation.

3.2. Hydrolytic and chemical stabilities

Hydrolytic and chemical stabilities of COFs materials were of vital importance for practical applications [60]. TpPa-2 reported in literature exhibited a high stability in water, acid and base due to the irreversible enol-to-keto tautomerization in TpPa-2 synthesis [34,35]. In order to further evaluate the practicability of TpPa-2(MW) and thus expand its potential application in water treatment, stabilities of TpPa-2(MW) in various solutions were extensively investigated via immersion test in other liquids involving organic solvent (n-hexane) and natural seawater. The results were illustrated in Fig. 6.

As seen in Fig. 6a, various TpPa-2(MW)-containing solutions exhibited distinguished colors and states, which depended on the inherent nature in terms of density and ionic strength of solvents. However, there was little change in color and state with increasing immersion period of 1, 3 and 7 days, and the dried TpPa-2(MW) samples after immersion test possessed an identical color with the as-synthesized TpPa-2(MW) (Fig. S3). SEM images showed that after immersion period of 7 days, the dried TpPa-2(MW) samples from various solutions still presented a specifically spherical and flower-like structure (Fig. 6b, Fig. S4), indicating an excellent structural stability of TpPa-2(MW). FTIR spectra showed that there was no extra or missing peak in comparison with the as-synthesized TpPa-2(MW) (Fig. 6c), indicating its inherently chemical stability due to the strongly linked covalent bonds between the starting materials via the irreversible enol-to-keto tautomerism [22,34,35]. Furthermore, PXRD measurements showed that the position and intensity of all peaks remained unchangeable, demonstrating its extraordinary stability of crystalline structure without crystalline-amorphous transition. All the measurements illustrated that the TpPa-2(MW) performed exceptionally hydrolytic and chemical stabilities in all the testing solutions including organic solvent and natural seawater, which would lay technical foundation for diverse aqueous applications such as wastewater treatment, seawater desalination and element extraction from seawater using membrane technology.

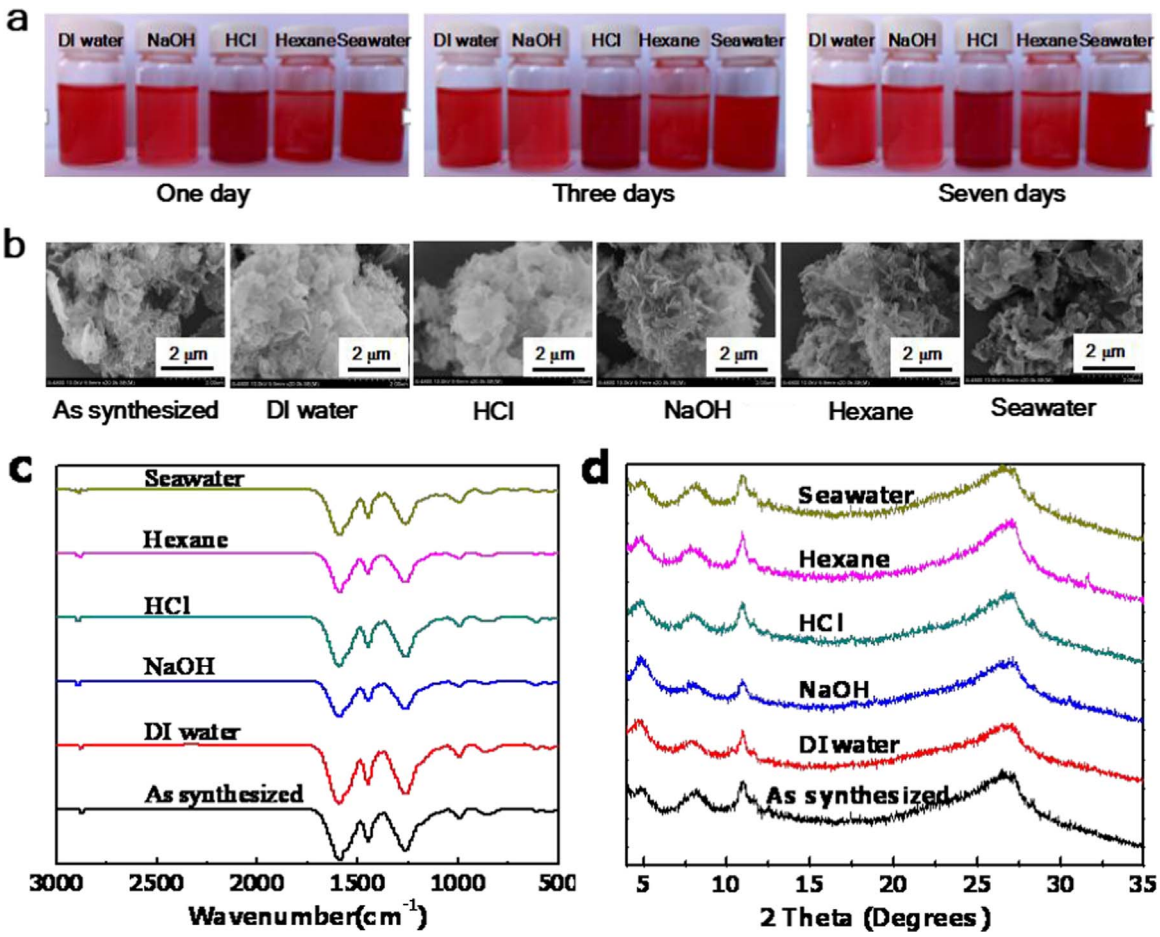

Fig. 6. Stability evaluation of TpPa-2(MW) in DI water, HCl solution, NaOH solution, n-hexane and seawater. (a) Digital photos of TpPa-2(MW) suspensions for 1, 3 and 7 days, respectively; (b) SEM images, (c) FTIR spectra, and (d) PXRD patterns of the dried TpPa-2(MW) samples after immersion test.

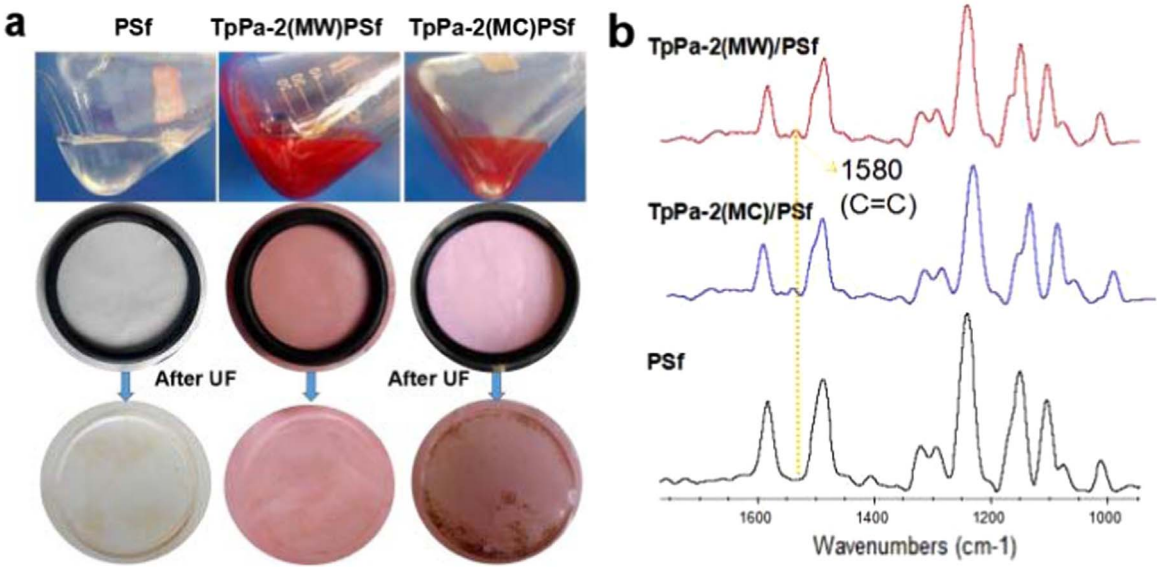

Fig. 7. Characterization of TpPa-2/PSf and PSf membranes. (a) comparison of color of the dope solutions, and the resulting membranes before and after filtrating HA solution; (b) FTIR spectra of PSf membrane, TpPa-2(MW)/PSf and TpPa-2(MC)/PSf membranes.

3.3. Characterization of TpPa-2-incorporated MMMs

In this study, we focused on the influence of two TpPa-2 prepared via microwave and mechanochemical approaches on the membrane structure and surface property, as shown in Fig. 7. The pure PSf membrane was evaluated for comparison. TpPa-2(MW) content in the casting solution was chosen at 0.2 wt% because extra TpPa-2(MW) tended to precipitate in the casting solution when its content was increased to 0.25 wt% (Fig. S5). As shown in Fig. 7a, the TpPa-2-containing dope solutions presented evenly red color, which were

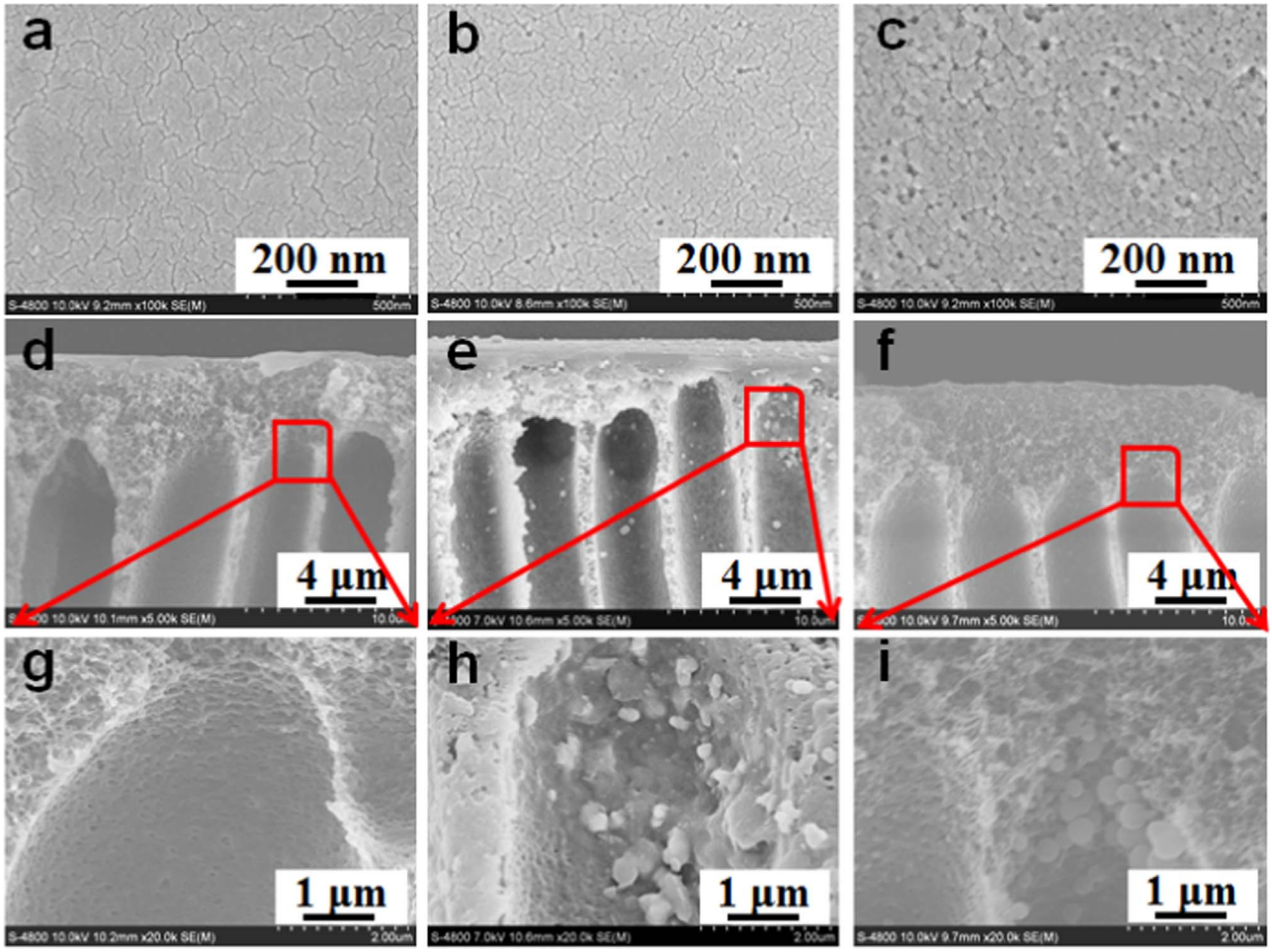

Fig. 8. SEM morphology of surfaces (a-c) and cross-section (d-i) of PSf membrane (a, d, g), TpPa-2(MW)/PSf membrane (b, e, h) and TpPa-2(MC)/PSf membrane (c, f, i).

remarkably different from the pure PSf dope solution. Pink surface was obtained for the resulting TpPa-2/PSf MMMs, while the pure PSf membrane showed white (Fig. 7a). Especially after the UF process of 8 h using HA as organic-foulant feed, the fouled TpPa-2(MW)/PSf and TpPa-2(MC)/PSf membranes still maintained pink (Fig. 7a), indicating a good operational stability and durability of TpPa-2 in the polymeric matrix. However, higher amount of HA was observed on the membrane surface for the TpPa-2(MC)/PSf membrane compared to the TpPa-2(MW)/PSf membrane, indicating an improved anti-fouling capacity of the TpPa-2(MW)/PSf membrane. It might be related to the membrane structure (Fig. 8), which will be discussed later. FTIR spectra showed that compared to the pure PSf membrane, an additional band at 1580 cm^{-1}, corresponding to C=C bond, was observed for both TpPa-2(MW)/PSf and TpPa-2(MC) membranes (Fig. 7b), confirming the successful incorporation of TpPa-2 in the membrane matrix.

SEM was performed to investigate the change in membrane morphology with the TpPa-2(MW) and TpPa-2(MC) incorporation. As seen in Fig. 8, with the same TpPa-2 content in the casting solution (0.2 wt%), the TpPa-2(MW)/PSf membrane exhibited a much smoother surface than TpPa-2(MC)/PSf membrane. As well known, smooth surface is necessary for the improvement in anti-fouling property for a membrane [61]. Therefore, less fouling was accumulated on the surface of TpPa-2(MW)/PSf and pure PSf membranes than that of TpPa-2(MC)/PSf membrane (Fig. 6a). From the cross-sectional images in Fig. 8d-i, nanoparticles with a diameter of ca. 200 nm were uniformly embedded in both the TpPa-2(MW)/PSf and TpPa-2(MC)/PSf membranes, while the pure PSf membrane seemed neat, although a typically asymmetry structure consisting of a dense layer and a macro-void middle region with finger-like pores was observed for three membranes. Reduction in particle size of the TpPa-2(MW) and TpPa-2(MC) embedded in membranes was probably attributed to the exfoliation by the sonication–stirring operation during the casting solution preparation [60].

Other membrane properties such as hydrophilicity, water uptake, porosity and thickness were also investigated, as shown in Fig. 9. The incorporation of TpPa-2 led to an obvious reduction in water contact angle from 90.1° (pure PSf membrane) to 77.4° and 69.2° (TpPa-2(MW)/PSf and TpPa-2(MC)/PSf membranes, respectively), indicated an improvement in the surface hydrophilicity of the TpPa-2-incorpo-

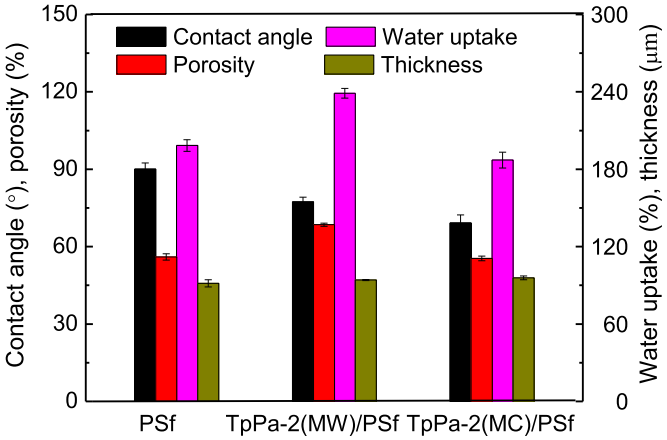

Fig. 9. Membrane properties of PSf, TpPa-2(MW)/PSf and TpPa-2(MC)/PSf membranes.

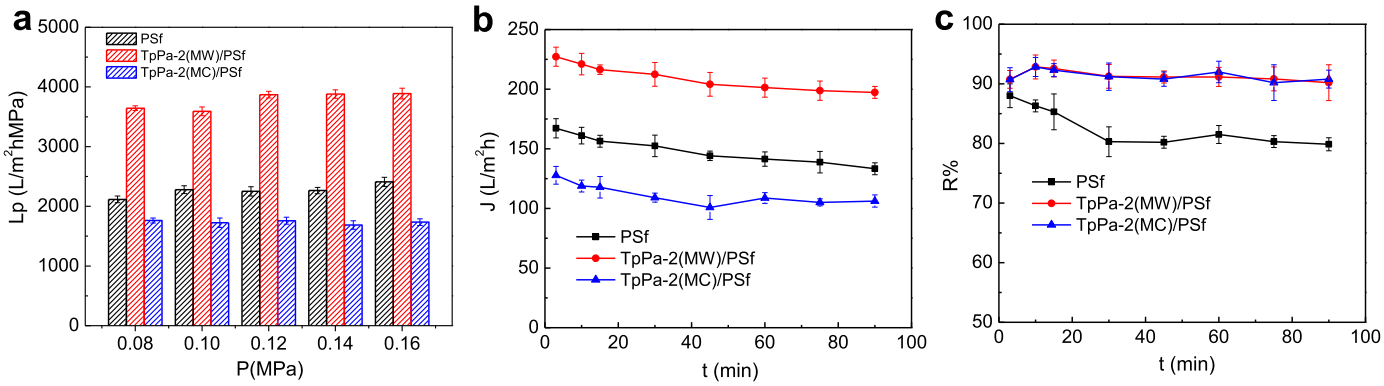

Fig. 10. Water transport property and separation performance of TpPa-2(MW)/PSf, TpPa-2(MC)/PSf and PSf membranes. (a) Pure water permeability, (b-c) water flux and HA rejection in filtrating 5 mg/L HA solution at 0.1 MPa, respectively.

rated MMMs. This might be related to the introduction of hydrophilic imino group (-N-H) in TpPa-2 into the membrane matrix. Besides, the difference in membrane thickness (91.5–95.8 μm) was statistically insignificant for three membranes. However, the water uptake and porosity of the TpPa-2(MW)/PSf membrane were much higher than those of both TpPa-2(MC)/PSf and pure PSf membranes. These distinct physical-chemistry properties for three membranes were attributed to the different TpPa-2 incorporation, which might exert significant influence on the separation performance of TpPa-2-incorporated MMMs.

3.4. Ultrafiltration performance and separation mechanism of TpPa-2-incorporated MMMs

In order to explore the contributions of TpPa-2 synthesized by different methods to the membrane performance, the water transport property of MMMs with the corporation of TpPa-2(MW) and TpPa-2(MC), respectively, was firstly investigated and the results are shown in Fig. 10a. For comparison, the pure PSf membrane was also tested. The TpPa-2(MW)/PSf membrane exhibited a significantly enhanced pure water permeability of approximately 3775 L/m^{2}hMPa, with an increase rate of 67% compared to the pure PSf membrane. On the contrary, when TpPa-2(MC) was used as filler with a same content, the resulting MMMs showed a much lower pure water permeability of only 1733 L/m^{2}hMPa. Based on the membrane characterization (Figs. 4 and 9), it was speculated that the major contribution to the improvement in the water transport capacity might be the improved membrane properties such as higher surface hydrophilicity and water uptake of the MMMs due to the incorporation of TpPa-2(MW), which was consistent with the previous study on MOFs-based MMMs [62,63].

It is clear that TpPa-2 prepared using different methods played distinct roles in water transport capacity of MMMs, demonstrating the significance of the TpPa-2 structure and properties such as particle size, S_{BET} and agglomerative tendency. According to the larger particle size and broader distribution of TpPa-2(MC) (Fig. 3d and Fig. 4a), bulk accumulation of TpPa-2(MC) in the casting solution might occur due to the high agglomerative tendency, leading to two opposite effects on the water permeability of MMMs. On one hand, TpPa-2(MC) accumulation resulted in a rougher membrane surface and thus the water contact angle was lowered to 69.2° (Fig. 9), which was supposed to enhance the water permeability. On the other hand, bulky TpPa-2(MC) was responsible for the partial pore blockage of MMMs, which was confirmed by the decreased water uptake and porosity (Fig. 9), leading to a largely increased mass resistance toward water molecules. To verify the impact of TpPa-2(MC) on the water transport capacity, we measured the pore size of membranes based on the bubble pressure method and the results were shown in Table S1. It can be found that the measured pressures of bubble point were 1.78, 2.42 and 1.42 bar for the pure PSf, TpPa-2(MC)/PSf and TpPa-2(MW)/PSf membranes, respectively, indicating that the largest pores of TpPa-2(MC)/PSf membrane were smaller than those of TpPa-2(MW)/PSf and PSf membranes, probably due to the pore blocking. It suggested the highest mass resistance of the TpPa-2(MC)/PSf membranes. Therefore, the TpPa-2(MC)/PSf membranes exhibited a poor water flux, which was even lower than that of pure PSf membranes. Moreover, the higher agglomerative tendency of TpPa-2(MC) might aggravate the pore tortuosity which also can lower the water transport property.

We next studied the separation efficiency of various membranes including TpPa-2(MW)/PSf, TpPa-2(MC)/PSf and pure PSf membranes for purifying organic foulant solution (5 mg/L HA) at 0.10 MPa. Fig. 10bc present the water flux (J) and HA rejection (R) as a function of filtration time. The water flux of membranes followed a similar profile as the pure water permeability that TpPa-2(MW) enhanced the flux while TpPa-2(MC) lowered the flux (Fig. 10b). For example, TpPa-2(MW)/PSf membrane yielded obviously improved initial and steady water fluxes of approximately 230 and 200 L/m^{2}h, respectively, with the corresponding increase rates of 35% and 54% compared to the pure PSf membranes (170 and 130 L/m^2 h). More importantly, the HA rejection of TpPa-2(MW)/PSf membrane was also enhanced and maintained over 90% during the whole filtration process, with an increase rate of 14% compared to the pure PSf membrane. It might be due to the pore diameter in nanoscale (~1.41 nm) of TpPa-2(MW) (Fig. 5c). These results prove that our TpPa-2(MW)/PSf membrane features both improved water permeability and rejection, breaking the intrinsic trade-off effect between permeability and selectivity of a polymer membrane. It also indicated the better compatibility between TpPa-2(MW) and PSf polymer due to their organic nature. In addition, we also observed a higher HA rejection for TpPa-2(MC)/PSf membrane, which was similar to that of TpPa-2(MW)/PSf membrane, indicating the effect of micro-pores in TpPa-2 materials on the effective retention of organic foulant.

Based on the material structure and separation efficiency, we proposed a phase inversion mechanism for the TpPa-2(MW)-incorporated MMMs to understand the effectiveness of TpPa-2(MW) in MMMs and the synchronous improvements in water permeability and HA rejection with the assistance of TpPa-2(MW). As well known, immersion of the casting film into water (coagulation bath) is a demixing process, where nuclei of a polymer-poor phase continue to grow with the continuation of the solvent and non-solvent exchange until the polymer concentration at their limits becomes too high, and solidification occurs [46]. As shown in Fig. 11, the incorporation of TpPa-2(MW) could effectively facilitate the water molecules (non-solvent) into the casting film to accelerate the exchange rate between DMAc (solvent) and water (non-solvent) due to the relatively hydrophilic nature and nanoporous structure of TpPa-2(MW), leading to an instantaneous demixing. As a result, compared to the slow demixing of the pure PSf membrane, instantaneous demixing of the TpPa-2(MW)/PSf casting film favors to the rapid formation of water channels

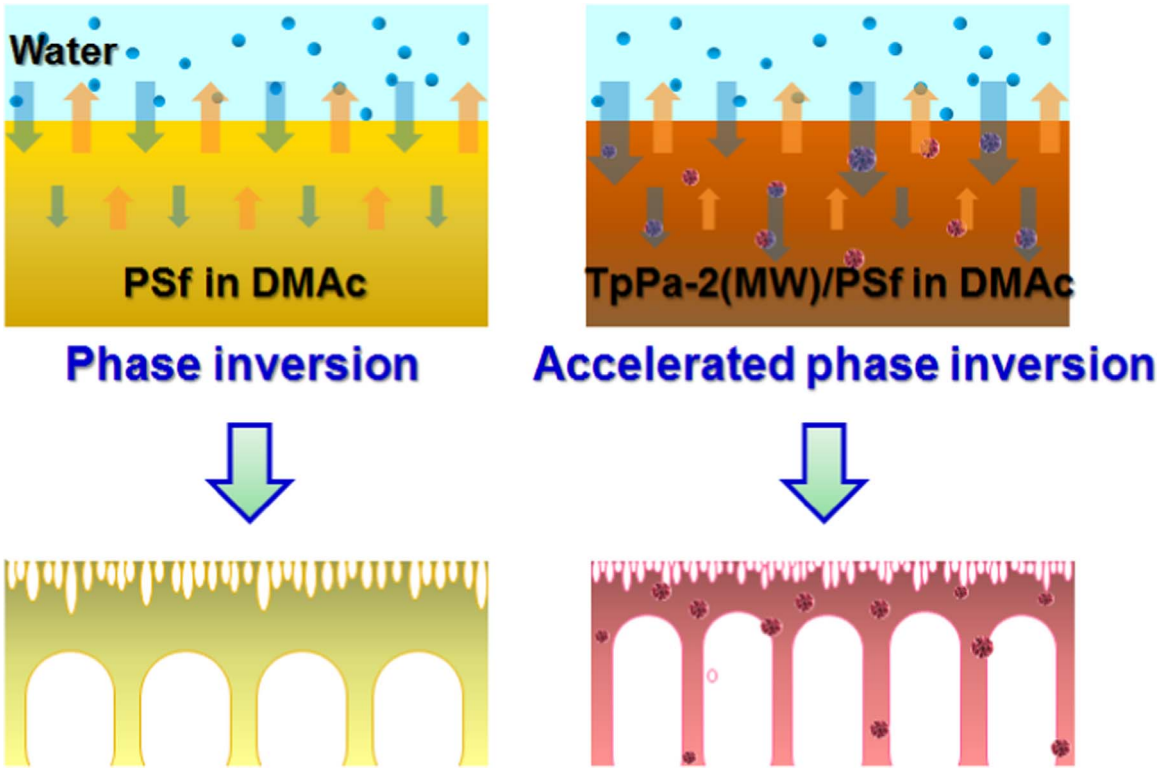

Fig. 11. Schematic diagram of the proposed phase inversion mechanism and the resulting membrane structure for the synchronous improvements in water permeability and HA rejection via incorporating TpPa-2(MW) into the membrane matrix.

(pores) with larger number and more uniform size distribution on the skin layer, and an improved porous structure with higher porosity and more finger-like pores in the macrovoids section (confirmed by characterization, Fig. 8 and Fig. 9). Therefore, the water flux is significantly enhanced with the aid of TpPa-2(MW) incorporation. Moreover, pores with even distribution and small size on the skin layer of TpPa-2(MW)/PSf membrane contributes to the high retention of organic foulant, leading to synchronous improvements in water permeability and HA rejection via incorporating TpPa-2(MW) into the membrane matrix. However, the lowered water flux and increased HA rejection were observed after incorporating TpPa-2(MC), which might be related to membrane pore block due to the severe agglomeration of TpPa-2(MC) in the membrane matrix.

3.5. Comparison with other MMMs for ultrafiltration

The strategy to improve separation performance by incorporating different fillers for the MMMs fabrication has great developed recently. Hereby we comprehensively summarized several representative MMMs for ultrafiltration in Table 1. It should be noted that the direct quantitative comparison on the separation performance is quite difficult due to the difference in polymeric material, filler type and content, feed type as well as filtrating conditions among different studies. Compared to state-of-the-art MMMs, our MMMs with incorporation of an ultralow amount (0.2 wt%) of TpPa-2(MW) showed significant advantages on the pure water permeability, water flux and solute rejection for ultrafiltration, indicating that this new generation COFs-based MMMs would be high performance, resource saving and cost-effective.

4. Conclusions

In summary, COFs were the first time to be used to prepare MMMs for water purification. The elaborately selected TpPa-2 was further proved to possess extensive stability in complicated water environments, which would lay technical foundation for diverse aqueous applications. To improve its practicability in MMMs, it was synthesized by convenient and effective microwave (MW) method within minutes. Under an optimal microwave condition, the resultant TpPa-2(MW) was endowed with much higher S_{BET} (535.2 m^2/g), smaller particle size and less agglomeration tendency than its counterparts obtained by mechanochemical method.

TpPa-2 was blended with PSf material to prepare MMMs. Influence of two TpPa-2 prepared via microwave and mechanochemical approaches on the membrane structure, surface property and separation performance was investigated. The results revealed that TpPa-2(MW)/PSf membrane showed much smoother membrane surface, higher porosity, higher water transport property and separation performance than TpPa-2(MC)/PSf and pure PSf membranes. With the same content of 0.2 wt% of TpPa-2, the TpPa-2(MW)/PSf membrane exhibited a significantly enhanced pure water permeability of approximately 3775 L/m^2 h MPa, with an increase rate of 67% compared to the PSf membrane. On the contrary, TpPa-2(MC)/PSf membrane showed a decreased pure water permeability of only 1733 L/m^2 h MPa. For the separation efficiency for purifying organic foulant solution (5 mg/L HA) at 0.10 MPa, the water flux of membranes followed a similar profile as the pure water permeability. Meanwhile, the HA rejection of both membranes was enhanced and maintained over 90% during the whole filtration process, proving the better compatibility between COFs fillers and polymeric matrices. Accordingly, a membrane forming mechanism was proposed to understand the synchronous improvements in water permeability and HA rejection for the TpPa-2(MW)/PSf membrane. Compared to state-of-the-art MMMs, our TpPa-2(MW)-incorporated MMMs featured both improved water permeability and rejection, breaking the intrinsic trade-off effect between permeability and selectivity of a polymer membrane, indicating that this new generation COFs-based MMMs would be high performance, resource saving and cost-effective.

Table 1
Comparison of separation performance of MMMs for ultrafiltration in literature and this study.

Mixed matrix membrane			Pure water filtration		Filtration text				Ref.
Polymer	Filler	Contents (wt%)	Lp (L/m^2 h bar)	Increase rate (%)	Feed	Operation pressure (Bar)	J (L/m^2 h)	R (%)	
PSf	TpPa-2(MW)	0.2	377.5	67.0	5 mg/L HA	1.0	200.1	92.0	This work
PSf	TpPa-2(MC)	0.2	173.3	−23.5	5 mg/L HA	1.0	112.0	91.6	This work
PSf	P(H-M-A)	0.5	580.0	142.1	5 mg/L HA	1.0	140.1	78.0	59
PVDF	TiO_2-PC-20	/ [a]	108.1	22.3	2 mg/L HA	0.4	31.2	/	9
PVDF	TiO_2-P25	/	94.3	6.8	2 mg/L HA	0.4	23.3	/	9
PVDF	TiO_2-X500	/	147.0	66.6	2 mg/L HA	0.4	53.3	/	9
PVDF	PDA	4.5	46.1	548.0	1 g/L BSA	1.0	11.2	32.2	63
PAN	MWCNTs	0.3		/	0.33 g/L Dextran	2.0	54.0	88.5	11
PSf	CNT-COOHs	0.1	330.2	29.4	/	1.0	/	/	10
PSf	MWCNTs	0.2	229.0	22.1	1 g/L PEO	1.0	150.4	96.0	12
PSf	Bentonite	0.8	309.0	415.2	200 mg/L Crude oil	1.0	145.2	90.5	8
PSf	Silica	0.8	140.1	133.0	200 mg/L Crude oil	1.0	75.1	91.5	8
PAN	C300	1.0	260.5	62.8	Dextran	5.0	/	99.1	14
PAN	A100	1.0	235.2	46.9	Dextran	5.0	/	98.2	14
PAN	F300	1.0	180.4	12.5	Dextran	5.0	/	99.5	14

[a] Data were not given in literature.

Acknowledgment

This work was supported by NSFC (No. 21306178), Shandong Province Key Project (2014GHY115033), Qingdao applied basic research project (No. 15-9-1-21-jch) and China Postdoctoral Science Foundation funded project (No. 2016M600560).

Appendix A. Supporting information

Supplementary data associated with this article can be found in the online version at doi:10.1016/j.memsci.2016.12.039.

References

[1] M.A. Shannon, P.W. Bohn, M. Elimelech, J.G. Georgiadis, B.J. Marinas, A.M. Mayes, Science and technology for water purification in the coming decades, Nature 452 (2008) 301–310.
[2] D.L. Gin, R.D. Noble, Designing the next generation of chemical separation membranes, Science 332 (2011) 674–676.
[3] B. Van der Bruggen, M. Mänttäri, M. Nyström, Drawbacks of applying nanofiltration and how to avoid them: a review, Sep. Purif. Technol. 63 (2008) 251–263.
[4] B.D. Freeman, Basis of permeability/selectivity tradeoff relations in polymeric gas separation membranes, Macromolecules 32 (1999) 375–380.
[5] L.M. Robeson, The upper bound revisited, J. Membr. Sci. 320 (2008) 390–400.
[6] T.-S. Chung, L.Y. Jiang, Y. Li, S. Kulprathipanja, Mixed matrix membranes (MMMs) comprising organic polymers with dispersed inorganic fillers for gas separation, Prog. Polym. Sci. 32 (2007) 483–507.
[7] J. Yin, B. Deng, Polymer-matrix nanocomposite membranes for water treatment, J. Membr. Sci. 479 (2015) 256–275.
[8] S. Kumar, C. Guria, A. Mandal, Synthesis, characterization and performance studies of polysulfone/bentonite nanoparticles mixed-matrix ultra-filtration membranes using oil field produced water, Sep. Purif. Technol. 150 (2015) 145–158.
[9] Y. Teow, B. Ooi, A. Ahmad, Fouling behaviours of PVDF-TiO 2 mixed-matrix membrane applied to humic acid treatment, J. Water Process Eng. (2016). http://dx.doi.org/10.1016/j.jwpe.2016.03.005.
[10] C.-F. de Lannoy, E. Soyer, M.R. Wiesner, Optimizing carbon nanotube-reinforced polysulfone ultrafiltration membranes through carboxylic acid functionalization, J. Membr. Sci. 447 (2013) 395–402.
[11] S. Majeed, D. Fierro, K. Buhr, J. Wind, B. Du, A. Boschetti-de-Fierro, V. Abetz, Multi-walled carbon nanotubes (MWCNTs) mixed polyacrylonitrile (PAN) ultrafiltration membranes, J. Membr. Sci. 403 (2012) 101–109.
[12] J.-H. Choi, J. Jegal, W.-N. Kim, Fabrication and characterization of multi-walled carbon nanotubes/polymer blend membranes, J. Membr. Sci. 284 (2006) 406–415.
[13] D. Qadir, H. Mukhtar, L.K. Keong, Synthesis and Characterization of Polyethersulfone/Carbon Molecular Sieve Based Mixed Matrix Membranes for, Water Treat. Appl. Procedia Eng. 148 (2016) 588–593.
[14] J.-Y. Lee, C.Y. Tang, F. Huo, Fabrication of porous matrix membrane (PMM) using metal-organic framework as green template for water treatment, Sci. Rep. 4 (2014).
[15] J. Duan, Y. Pan, F. Pacheco, E. Litwiller, Z. Lai, I. Pinnau, High-performance polyamide thin-film-nanocomposite reverse osmosis membranes containing hydrophobic zeolitic imidazolate framework-8, J. Membr. Sci. 476 (2015) 303–310.
[16] A.G. Fane, R. Wang, M.X. Hu, Synthetic membranes for water purification: status and future, Angew. Chem. Int. Ed. 54 (2015) 3368–3386.
[17] R. Zhang, S. Ji, N. Wang, L. Wang, G. Zhang, J.R. Li, Coordination-driven in situ self-assembly strategy for the preparation of metal–organic framework hybrid membranes, Angew. Chem. Int. Ed. 53 (2014) 9775–9779.
[18] A. Khan, I. Vankelecom, Metal organic framework containing mixed matrix membranes for gas separation: a different approach to Mmm preparation methods, Procedia Eng. 44 (2012) 106–107.
[19] L. Zhang, J. Xu, Y. Tang, J. Hou, L. Yu, C. Gao, A novel long-lasting antifouling membrane modified by bifunctional capsaicin-mimic moieties via in situ polymerization for efficient water purification, J. Mater. Chem. A 4 (2016) 10352–10362.
[20] Z. Kang, Y. Peng, Y. Qian, D. Yuan, M.A. Addicoat, T. Heine, Z. Hu, L. Tee, Z. Guo, D. Zhao, Mixed matrix membranes (MMMs) comprising exfoliated 2D covalent organic frameworks (COFs) for efficient CO_2 separation, Chem. Mater. 28 (2016) 1277–1285.
[21] K.A. Cychosz, A.J. Matzger, Water stability of microporous coordination polymers and the adsorption of pharmaceuticals from water, Langmuir 26 (2010) 17198–17202.
[22] A.P. Cote, A.I. Benin, N.W. Ockwig, M. O'Keeffe, A.J. Matzger, O.M. Yaghi, Porous, crystalline, covalent organic frameworks, Science 310 (2005) 1166–1170.
[23] X. Cao, Z. Qiao, Z. Wang, S. Zhao, P. Li, J. Wang, S. Wang, Enhanced performance of mixed matrix membrane by incorporating a highly compatible covalent organic framework into poly(vinylamine) for hydrogen purification, Int. J. Hydrogen Energy 41 (2016) 9167–9174.
[24] M. Shan, B. Seoane, E. Rozhko, A. Dikhtiarenko, G. Clet, F. Kapteijn, J. Gascon, Azine-linked covalent organic framework (COF)-based mixed-matrix membranes for CO_2/CH_4 separation, Chemistry 22 (2016) 14467–14470.
[25] H.M. El-Kaderi, J.R. Hunt, J.L. Mendoza-Cortés, A.P. Côté, R.E. Taylor, M. O'Keeffe, O.M. Yaghi, Designed synthesis of 3D covalent organic frameworks, Science 316 (2007) 268–272.
[26] J.R. Hunt, C.J. Doonan, J.D. LeVangie, A.P. Côté, O.M. Yaghi, Reticular synthesis of covalent organic borosilicate frameworks, J. Am. Chem. Soc. 130 (2008) 11872–11873.
[27] S.-Y. Ding, W. Wang, Covalent organic frameworks (COFs): from design to applications, Chem. Soc. Rev. 42 (2013) 548–568.
[28] E.L. Spitler, M.R. Giovino, S.L. White, W.R. Dichtel, A mechanistic study of Lewis acid-catalyzed covalent organic framework formation, Chem. Sci. 2 (2011) 1588–1593.
[29] Y. Du, K. Mao, P. Kamakoti, P. Ravikovitch, C. Paur, S. Cundy, Q. Li, D. Calabro, Experimental and computational studies of pyridine-assisted post-synthesis modified air stable covalent–organic frameworks, Chem. Commun. 48 (2012) 4606–4608.
[30] A. Bhunia, I. Boldog, A. Möller, C. Janiak, Highly stable nanoporous covalent triazine-based frameworks with an adamantane core for carbon dioxide sorption and separation, J. Mater. Chem. A 1 (2013) 14990–14999.
[31] L.A. Baldwin, J.W. Crowe, M.D. Shannon, C.P. Jaroniec, P.L. McGrier, 2D covalent organic frameworks with alternating triangular and hexagonal pores, Chem. Mater. 27 (2015) 6169–6172.
[32] U. Díaz, A. Corma, Ordered covalent organic frameworks, COFs and PAFs. From preparation to application, Coord. Chem. Rev. 311 (2016) 85–124.
[33] S. Duhovic, M. Dinca, Synthesis and electrical properties of covalent organic frameworks with heavy chalcogens, Chem. Mater. 27 (2015) 5487–5490.
[34] S. Kandambeth, A. Mallick, B. Lukose, M.V. Mane, T. Heine, R. Banerjee, Construction of crystalline 2D covalent organic frameworks with remarkable chemical (acid/base) stability via a combined reversible and irreversible route, J. Am. Chem. Soc. 134 (2012) 19524–19527.
[35] B.P. Biswal, S. Chandra, S. Kandambeth, B. Lukose, T. Heine, R. Banerjee, Mechanochemical synthesis of chemically stable isoreticular covalent organic frameworks, J. Am. Chem. Soc. 135 (2013) 5328–5331.
[36] U.K. Kharul, R. Banerjee, B. Biswal, H.D. Chaudhari, Chemically stable covalent organic framework (COF)-polybenzimidazole hybrid membranes: enhanced gas

separation through pore modulation, Chem. Eur. J. 22 (2016) 4695–4699.
[37] H. Wei, S. Chai, N. Hu, Z. Yang, L. Wei, L. Wang, The microwave-assisted solvothermal synthesis of a crystalline two-dimensional covalent organic framework with high CO_2 capacity, Chem. Commun. 51 (2015) 12178–12181.
[38] M.B. Gawande, S.N. Shelke, R. Zboril, R.S. Varma, Microwave-assisted chemistry: synthetic applications for rapid assembly of nanomaterials and organics, Acc. Chem. Res. 47 (2014) 1338–1348.
[39] E. Haque, C.M. Kim, S.H. Jhung, Facile synthesis of cuprous oxide using ultrasound, microwave and electric heating: effect of heating methods on synthesis kinetics, morphology and yield, CrystEngComm 13 (2011) 4060–4068.
[40] Y. Li, W. Yang, Microwave synthesis of zeolite membranes: a review, J. Membr. Sci. 316 (2008) 3–17.
[41] N.A. Khan, S.H. Jhung, Synthesis of metal-organic frameworks (MOFs) with microwave or ultrasound: rapid reaction, phase-selectivity, and size reduction, Coord. Chem. Rev. 285 (2015) 11–23.
[42] H. Guo, M. Wang, J. Liu, S. Zhu, C. Liu, Facile synthesis of nanoscale high porosity IR-MOFs for low-k dielectrics thin films, Microporous Mesoporous Mater. 221 (2016) 40–47.
[43] N.L. Campbell, R. Clowes, L.K. Ritchie, A.I. Cooper, Rapid microwave synthesis and purification of porous covalent organic frameworks, Chem. Mater. 21 (2009) 204–206.
[44] L.K. Ritchie, A. Trewin, A. Reguera-Galan, T. Hasell, A.I. Cooper, Synthesis of COF-5 using microwave irradiation and conventional solvothermal routes, Microporous Mesoporous Mater. 132 (2010) 132–136.
[45] J.H. Chong, M. Sauer, B.O. Patrick, M.J. MacLachlan, Highly stable keto-enamine salicylideneanilines, Org. Lett. 5 (2003) 3823–3826.
[46] J. Xu, Y. Tang, Y. Wang, B. Shan, L. Yu, C. Gao, Effect of coagulation bath conditions on the morphology and performance of PSf membrane blended with a capsaicin-mimic copolymer, J. Membr. Sci. 455 (2014) 121–130.
[47] J. Xu, X. Feng, P. Chen, C. Gao, Development of an antibacterial copper (II)-chelated polyacrylonitrile ultrafiltration membrane, J. Membr. Sci. 413 (2012) 62–69.
[48] Y. Tang, J. Xu, C. Gao, Ultrafiltration membranes with ultrafast water transport tuned via different substrates, Chem. Eng. J. 303 (2016) 322–330.
[49] P.-S. Shen, C.-M. Tseng, T.-C. Kuo, C.-K. Shih, M.-H. Li, P. Chen, Microwave-assisted synthesis of titanium dioxide nanocrystalline for efficient dye-sensitized and perovskite solar cells, Sol. Energy 120 (2015) 345–356.
[50] Y. Li, W. Yang, Microwave synthesis of zeolite membranes: a review, J. Membr. Sci. 316 (2008) 3–17.
[51] X. Wu, Z. Bao, B. Yuan, J. Wang, Y. Sun, H. Luo, S. Deng, Microwave synthesis and characterization of MOF-74 (M= Ni, Mg) for gas separation, Microporous Mesoporous Mater. 180 (2013) 114–122.
[52] A.B. Cairns, A.L. Goodwin, Structural disorder in molecular framework materials, Chem. Soc. Rev. 42 (2013) 4881–4893.
[53] Al.U. Ortiz, A. Boutin, A.H. Fuchs, Fo-X. Coudert, Investigating the pressure-induced amorphization of zeolitic imidazolate framework ZIF-8: mechanical instability due to shear mode softening, J. Phys. Chem. Lett. 4 (2013) 1861–1865.
[54] T.D. Bennett, A.K. Cheetham, Amorphous metal–organic frameworks, Acc. Chem. Res. 47 (2014) 1555–1562.
[55] M.R. Lohe, M. Rose, S. Kaskel, Metal–organic framework (MOF) aerogels with high micro-and macroporosity, Chem. Commun. (2009) 6056–6058.
[56] T.D. Bennett, D.A. Keen, J.C. Tan, E.R. Barney, A.L. Goodwin, A.K. Cheetham, Thermal amorphization of zeolitic imidazolate frameworks, Angew. Chem. Int. Ed. 50 (2011) 3067–3071.
[57] M.G. Goesten, E. Stavitski, J. Juan-Alcaniz, A. Martinez-Joaristi, A.V. Petukhov, F. Kapteijn, J. Gascon, Small-angle X-ray scattering documents the growth of metal-organic frameworks, Catal. Today 205 (2013) 120–127.
[58] T.D. Bennett, P. Simoncic, S.A. Moggach, F. Gozzo, P. Macchi, D.A. Keen, J.-C. Tan, A.K. Cheetham, Reversible pressure-induced amorphization of a zeolitic imidazolate framework (ZIF-4), Chem. Commun. 47 (2011) 7983–7985.
[59] T.D. Bennett, P.J. Saines, D.A. Keen, J.C. Tan, A.K. Cheetham, Ball-milling-induced amorphization of zeolitic imidazolate frameworks (ZIFs) for the irreversible trapping of iodine, Chem. Eur. J. 19 (2013) 7049–7055.
[60] Z. Kang, Y. Peng, Y. Qian, D. Yuan, M.A. Addicoat, T. Heine, Z. Hu, L. Tee, Z. Guo, D. Zhao, Mixed matrix membranes (MMMs) comprising exfoliated 2D covalent organic frameworks (COFs) for efficient CO_2 separation, Chem. Mater. 28 (2016) 1277–1285.
[61] J. Xu, X. Feng, J. Hou, X. Wang, B. Shan, L. Yu, C. Gao, Preparation and characterization of a novel polysulfone UF membrane using a copolymer with capsaicin-mimic moieties for improved anti-fouling properties, J. Membr. Sci. 446 (2013) 171–180.
[62] C. Kong, T. Kamada, T. Shintani, M. Kanezashi, T. Yoshioka, T. Tsuru, Enhanced performance of inorganic-polyamide nanocomposite membranes prepared by metal-alkoxide-assisted interfacial polymerization, J. Membr. Sci. 366 (2011) 382–388.
[63] J.Y. Lee, Q. She, F. Huo, C.Y. Tang, Metal–organic framework-based porous matrix membranes for improving mass transfer in forward osmosis membranes, J. Membr. Sci. 492 (2015) 392–399.